Biodegradable porous polylactic acid film as a separator for supercapacitors

Biodegradable porous polylactic acid film as a separator for supercapacitors

ElifVargun[1,2]|Kadir Ozaltin[1]|Haojie Fei[1]|Evghenii Harea[1]|Jarmila Vilcáková[1]|Natalia Kazantseva[1]|Petr Saha[1]

[1]Centre of Polymer Systems, Tomas Bata University in Zlín, Zlín, Czech Republic

[2]Department of Chemistry, Mugla Sitki Kocman University, Mugla, Turkey

Correspondence – Elif Vargun, Centre of Polymer Systems, Tomas Bata University in Zlín, Tř. T. Bati 5678, 760 01, Zlín, Czech Republic. Email: elifvargun@gmail.com

Abstract

A porous polylactic acid (PLA) film was investigated as a separator for supercapacitors (SCs) and compared with commercial separators, for example, NKK-MPF30AC and Celgard 2400. The porous PLA film was fabricated via a facile phase inversion method, and the cross-sectional scanning electron microscope images of the PLA separator film exhibited highly porous interconnected morphology for ion diffusion. The surface modification of separators was performed by radio frequency (RF) air plasma to improve wettability. The plasma modification enhanced the water uptake and swelling properties of the separators and decreased the water contact angles of PLA and Celgard 2400 films. The mechanical and dielectric properties of separators were also studied. The ionic conductivities of RF-PLA in 1 M H_2SO_4 and 1 M Na_2SO_4 were found to be 1.1 x 10^{-1} S/cm and 0.6 X 10^{-2} S/cm at room temperature, respectively. The electrochemical impedance spectroscopy of the RF-PLA SCs showed the lowest solution resistance and internal resistance.

KEYWORDS

biodegradable, biopolymers and renewable polymers, electrochemistry, polyelectrolytes

1 | INTRODUCTION

Supercapacitors (SCs) are promising energy storage devices in various applications requiring high power density, such as portable devices, hybrid power systems for electric vehicles, aircraft vehicles (UAVs, UGVs, etc.), and smart grids.[1-3] The main components of SCs are electrodes (cathode, anode), electrolytes, and separators. To improve the performance of SCs, extensive work has been focused on increasing the specific capacitance of electrodes[4] and widening the cell voltage by newly developed electrolytes and separators. [5,6] Synthetic polymer-based solid electrolytes or separators have been widely used in SCs, and their biodegradable alternatives from renewable sources have always been sought after because of environmental and economic concerns.[7,8]

The major advantages of polymer electrolytes and separators are that they are flexible, easy to fabricate, free of leakage, nonvolatile, and low flammable. [9] Much attention has been given to the development of high performance SCs by enhancing the ionic conductivity and chemical and electrochemical stability of polymer electrolytes and separators. The usage of different polymers or polymer blends that are well matched to electrodes enables one to widen the potential window and

broaden the operating temperature range. The most widely used hydrogel electrolyte separator is the poly(vinyl alcohol) (PVA) for flexible SCs. Wan and his coworkers prepared a flexible and self-healable PVA hydrogel electrolyte crosslinked by hydrogen bonds for an SC with all-in-one configuration. [10] A flexible sandwich-structured SC with a PVA/H_3PO_4-soaked cotton fabric as the electrolyte matrix and separator was reported for potential applications in smart textiles and wearable electronics.[11] To improve the network structure and mechanical properties, cellulose/PVA composite gels are prepared as separators for quasi-solid state electrical double layer capacitors (EDLCs). Compared with the PVA gel, composite gels showed good cycling stability with capacitance retention of 88% after 1,500 cycles.[12]

A semi-interpenetrating polymer network (semi-IPN) based on poly(ethylene oxide) (PEO) and noncrosslinked nitrile butadiene rubber system has been reported for high thermal and dimensional stability. The produced semi-IPN membranes exhibit an operating temperature range of from -80 to 120°C, which is wider than that of the classical cellulose separator.[13] The SCs based on a porous polyacrylonitrile nanofibers separator[14] and a crosslinked quaternized poly(arylene ether sulfone) membrane[15] showed good cycle stability. These polymer electrolytes or separators are expected to meet the fundamental requirements to be ideal materials for energy storage devices with high energy/power density and good cycling stability. However, most of these materials are not biodegradable and environmentally friendly. Moreover, they are not manufactured from renewable sources.

Considering the environmental effects, biodegradable, and environmentally friendly polymer electrolytes/sepa-rators have been taken more attention in the design of SCs due to the abundance in nature, renewable sources, and low cost. A blend of chitosan (CS) and poly(ethylene glycol) (PEG) was used as a biodegradable polymer electrolyte for SCs.[16] Lithium perchlorate ($LiClO_4$)-doped plasticized blend exhibited a maximum conductivity of 1.1 X 10^{-4} S/cm and high coulombic efficiency. CS was also blended with starch and doped with $LiClO_4$,[17] and the fabricated SC showed a good electrochemical performance with a specific capacitance of 133 F/g. Another kind of biodegradable electrolyte was produced from corn starch, which was doped with lithium acetate and plasticized with glycerol.[18] The maximum ionic conductivity was improved to 1.04 X 10^{-3} S/cm.

Biomass-derived and bio-inspired materials have recently been used as both electrode and electrolyte in SCs, such as waste-bone,[19] eggshell,[20] lignin,[21] wood,[22] soybean leaf,[23] and kelp.[24] These bio-derived materials play an important role in sustainable energy storage systems and have not only unique mechanical and physicochemical properties but also a characteristic chemical structure; that is, they are rich in N, O, and S heteroatoms in their structures. Hence, the presence of these self-doped heteroatoms (especially O and N) is useful in electrolytes/separators for high performance SCs.

3D porous polymer separators facilitate ion conductivity. Hence, the innovative alternatives are attractive for the fabrication of porous polymer films. When compared with electrospinning, the phase inversion is a simpler, cheaper, and more efficient technique for the preparation of porous polymer membranes. The phase inversion method was used for the preparation of a mesoporous cellulose membrane in solid-state SCs by Zhao et al.[25] Poly(vinylidene fluoride) (PVDF) porous membranes as a separator for a symmetric SC were also fabricated by the phase inversion technique.[26] Another work on PVDF-ceramic composite based separators demonstrated that the phase inversion precipitation technique is a feasible and scalable method for the fabrication of these porous polymer composite membranes.[27]

The aim of this study was to prepare porous polylactic acid (PLA) based biodegradable separators for SCs. To this end, we applied the phase inversion technique to fabricate a highly porous structure of a

PLA film: we used PEG 4000 as the sacrificial polymer and constructed interlinked PLA with porous morphology by removing the sacrificial polymer. The separator films were subjected to radio frequency (RF) air plasma treatment for 60 s to improve wettability. In addition, we compared the chemical and electrochemical properties of the porous PLA separator with those of typical commercial separators, namely, NKK-MPF30AC-100 (cellu-losic separator paper) and Celgard 2400 (polypropylene-based separator).

2 | EXPERIMENTAL

2.1 | Materials

PLA 4,032 D in pellet form was purchased from Nature Works (Blair, NE, melt density: 1.08 g/ml at 230°C, specific gravity: 1.24 kg/m^3, semicrystalline). PEG (BioUltra, mp: 58-61°C and fp: 229°C, clear, colorless) with a molecular weight of 4,000 was purchased from Sigma-Aldrich, Germany. Dichloromethane (99.8%, density: 1.325 g/ml at 25° C, Sigma-Aldrich) solvent was used as received. Carbon black (Super-P, conductive, 99+% [metals basis]) was purchased from Alfa Aesar, and commercial separators NKK-MPF30AC (cellulose based, 89 µm, 30 g/m^2, Nagano-ken, Japan) and Celgard 2400 (polypropylene based, thickness: 24 µm, area: 0.6 m^2) were used as reference separators.

2.2 | Fabrication of a porous PLA separator

The phase inversion method was used to produce a PLA film with porous structure (Figure 1).

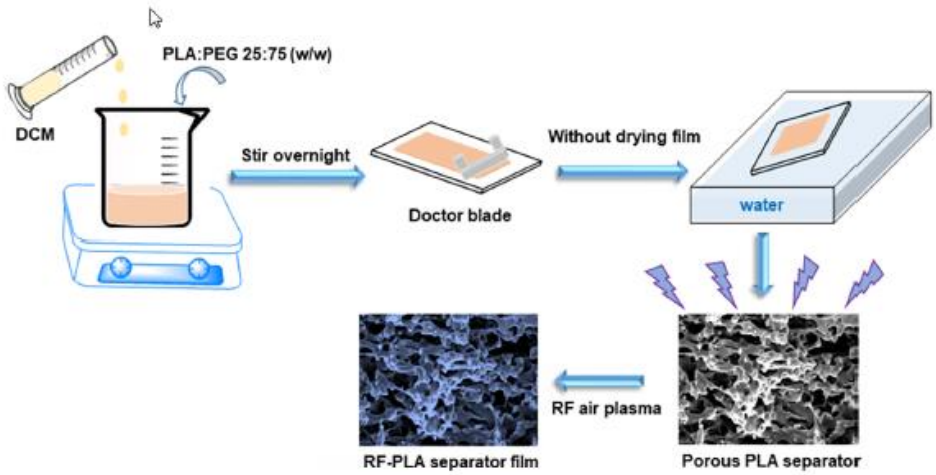

FIGURE 1 Fabrication technology of PLA-based separator: preparation of porous PLA separator by phase inversion technique; surface treatment by RF air plasma [Color figure can be viewed at wileyonlinelibrary.com]

Briefly, porous films were prepared by a solution casting-porogen leaching technique. However, instead of using NaCl salt or particulates, we used PEG 4000 itself as a sacrificial polymer for pore generation. The weight ratio of PLA to PEG was 25:75. The PLA and PEG 4000 were dissolved in dichloromethane, and the solution concentration was adjusted to 0.143 g/ml. The viscous polymer blend (PLA and PEG4000) solution was poured onto a clean glass plate and spread by the doctor-blade

method as 73 mm x 97 mm dimensions films. Then the wet films that spread on glass plates were soaked in deionized water without completely drying it. The polymer blend film peeled off the glass plate in deionized water bath spontaneously and became a freestanding film. The deionized water is solvent for PEG 4000, but it is nonsolvent for PLA. Hence, the phase inversion process was started for the PLA transformation from a liquid phase to solid phase and the dissolution of PEG 4000 in water started simultaneously for obtaining highly porous films. The films were placed in deionized water for 48 hr at 25° C for leaching out the PEG porogens, and water was changed every 12 hr. The full removal of PEG porogens resulted in the formation of an interconnected PLA skeleton with highly porous structure. The films were dried at 50° C in an oven for 12 hr. The dimensions of the films did not change after drying process and RF plasma treatment.

The separator films were exposed to RF plasma treatment for 60 s to increase their hydrophilicity by including hydrophilic functional groups (hydroxyl, carboxyl) on the surface, as well as increasing the surface area by physical etching. RF plasma was generated by a PICO (Diener, Germany) plasma reactor with a power of 50 W and frequency of 13.56 MHz. Air was used as a carrier gas with a flow rate of 20 sccm under the chamber pressure of 50 Pa.

2.3 | Characterization of separator films

2.3.1 | Morphology of separator films: SEM analysis

The morphology of the separator films was investigated by a NANOSEM 450 (FEI) scanning electron microscope (SEM) operated at 5 kV under a pressure of 90 Pa. The films were frozen in liquid nitrogen and then broken into two parts to reveal the lateral section in its original state. Images were taken at magnifications of x5k and x10k.

2.3.2 | Water contact angle measurements

The wettability behavior of the separator films was investigated by the sessile drop method via SEE System (Advex Instruments, Czech Republic) equipped with a CCD camera to reveal its surface hydrophilicity. Ten separate distilled water droplets of 5 pl in volume were applied to each film to obtain the average water contact angle value (Qw) at 23° and 62% relative humidity.

2.3.3 | Water absorption test

Water uptakes of PLA, NKK, and Celgard 2400 separators with and without RF-plasma treatment were measured by immersing the samples into deionized water at room temperature until swelling equilibrium was attained. The weight gain of the separator films was recorded as a function of time, and the equilibrium swelling ratio (SR) of the films was calculated according to Equation (1):

$$\mathrm{SR(wt\%)} = \frac{W_t - W_0}{W_0}.100, \qquad (1)$$

where W_t is the weight of a wet sample at equilibrium after a certain period of immersion in water and W_0 is the weight of the fully dried sample.

2.3.4 | Dielectric relaxation spectroscopy

Dielectric measurements were performed as frequency sweeps in the range 0.1-10 MHz at ambient temperature at a measuring voltage amplitude of i V using a Novocontrol impedance analyzer (Germany) on samples in the form of 10-mm diameter discs with a thickness of about 20 µm. AC conductivity of separators before and after plasma treatment was calculated using the measured dielectric loss parameter (Ɛ") by applying Equation (2):

$$\sigma_{AC} = \varepsilon_0 \omega \varepsilon'', \qquad (2)$$

where ϵ_0 is permittivity free space (8.854 x 10 $^{-12}$ F·m) and ω = 2πf is the angular frequency.[28]

2.3.5 | Mechanical (tensile) test

All films were tested and compared in terms of their mechanical properties. Samples were carefully cut using a 10 x 80 mm^2 press knife. Tensile test was carried out according to the methodology described in Reference [29] using a Testometric M350 tensile machine (Testometric Company, Ltd. UK.) under ambient conditions with crosshead speeds of 50 mm/min. The stress-strain parameter values were taken from an average of five specimens.

2.4 | Electrochemical characterization of separator films

2.4.1 | Ionic conductivity

All separators were immersed in 1 M aqueous electrolyte solutions of sulfuric acid (H_2SO_4) and sodium sulfate (Na_2SO_4). The ionic conductivity of the samples was measured by electrochemical impedance spectroscopy (EIS) by placing the samples between two round stainless steel plates. The impedance data were collected by Autolab PGSTAT128N (Metrohm, Netherlands) in the frequency range from 0.1 to 100 kHz with amplitude of 10 mV. The conductivity of the samples was calculated by following formula:

$$\sigma = \frac{l}{R_b A} \qquad (3)$$

where σ is the ionic conductivity, R_b is the bulk resistance, *l* is the thickness of a separator, A is the contact area between the separator and the stainless steel plate.[30,31]

2.4.2 | Electrochemical performance in a symmetric activated carbon cell

The SC cells were fabricated using commercial activated carbon (DARCO, 100 mesh particle size, powder). Super-P was added as a conducting additive, and poly-tetrafluoroethylene (PTFE, 60wt% dispersion in H_2O) was used as a binder material. The composite: Super-P: binder ratio was maintained at a value of 80:10:10. The electrode films with diameter of 4.5 mm were pressed onto titanium meshes. The electrodes were dried at 80° C in an oven overnight. Symmetric cells were fabricated in 1 M aqueous electrolyte solutions of sulfuric acid (H_2SO_4), using different separators (NKK-MPF30AC, PLA, Celgard 2400, and their RF-plasma treated samples) between two stainless steel collectors in a Teflon Swagelok system. Cyclic voltammograms (CVs) and EIS(frequency range of 0.1 Hz-100 kHz) measurements were performed using an Autolab PGSTAT128N potentiostat (Metrohm, Netherlands).

Galvanostatic charge-discharge cycling of the cells was conducted over a potential range of 0-0.8 V using a battery testing equipment (BCS-810, Bio-Logic) under a constant current density in 1 A/g at room temperature.

3 | RESULTS AND DISCUSSION

Supercapacitor separators must perform some important tasks such as ensuring high ionic conductivity, nonconductive property, compensating the pressure and volume changes, and resistance to chemicals. Porous polymer membranes are promising separator materials for SCs in view of their enhanced electrolyte uptake, ease of fabrication, and mechanical robustness. Therefore, porous polymer separators, particularly cost-effective and environmentally friendly ones, have been studied more extensively. The main limitation of polymer separators is their low surface energy, which results in poor wettability. A plasma surface modification technique was used to circumvent this limitation by controlling the surface functionality and surface energy of polymers. The prepared PLA films and commercial separators (NKK and Celgard 2400) were subjected to RF plasma treatment to increase the number of hydrophilic groups and to improve surface wettability. The effect of RF plasma on separator films was tested by water uptake and water contact angle measurements. The tensile properties of films were determined, and the pore structure morphologies were examined by SEM. The ionic conductivity of a separator in electrolyte, which is one of the most important parameters for its application in SCs, was measured in two most common aqueous electrolytes. Several symmetric SCs were assembled using different separators. The performance of these separators in SCs was studied through their electrochemical properties.

3.1 | SEM analysis

After the RF-treatment of separator films, their topographies and cross section morphologies were investigated by SEM analysis. The SEM images of an RF-NKK film in Figure 2a,b clearly show that the cellulose separator is composed of nonoriented interlinked cellulose fibers. The porous structure is formed by a fibrous network with disordered arrangement. Hence, the porous micromorphology of the RF-NKK separator provides an efficient ion transport pathway. During the fabrication of a PLA separator by the phase inversion technique, the removal of PEG 4000 porogens from the PLA matrix resulted in a sponge-like structure, as shown in the crosssectional SEM images (Figure 2d,e). A highly porous interconnected structure can facilitate the ion diffusion through the channels and provide sufficient space to uptake liquid electrolytes. However, the cross-sectional SEM images of the RF-Celgard 2400 separator film exhibited nonporous monolithic morphology, which is micromorphology of the RF-NKK separator provides an efficient ion transport pathway. During the fabrication of a PLA separator by the phase inversion technique, the removal of PEG 4000 porogens from the PLA matrix resulted in a sponge-like structure, as shown in the crosssectional SEM images (Figure 2d,e). A highly porous interconnected structure can facilitate the ion diffusion through the channels and provide sufficient space to uptake liquid electrolytes. However, the cross-sectional SEM images of the RF-Celgard 2400 separator film exhibited nonporous monolithic morphology, which is not feasible for SC separators (Figure 2g,h). The ionic motion is directly affected by the pore structure of the separator,

so porous systems are essential for the Celgard 2400 separator film even if its wettability was improved by surface treatment.

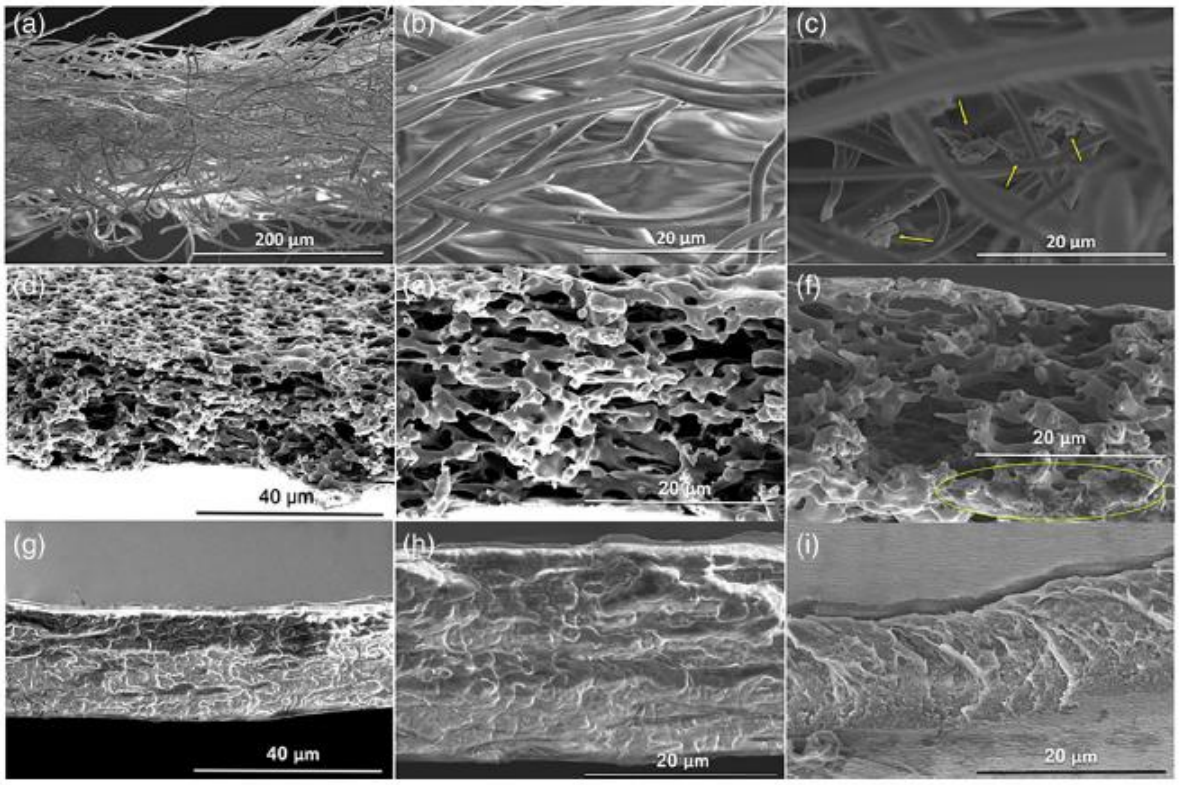

FIGURE 2 SEM images (a, b, and c) for RF-NKK-MPF30AC; (d, e, and f) for RF-PLA; (g, h, and i) for RF-Celgard 2400 separators [Color figure can be viewed at wileyonlinelibrary.com]

The chemical and mechanical stabilities of RF-NKK (Figure 2c), RF-PLA (Figure 2f), and RF-Celgard (Figure 2i) separators were investigated by SEM after electrochemical measurements. All separators maintained their structural integrity mechanically and none of them showed deformations after electrochemical measurements. It can be seen that some part of the activated carbon penetrated into the RF-NKK separator (Figure 2c). The permeation of the small amount of active material is due to the fibrous network structure of cellulose fibers. The SEM analysis of RF-PLA separator revealed that the active materials stayed on only the surface of the film and no penetration of activated carbon through the film (Figure 2f). The morphological changes were not observed for RF-Celgard film after electrochemical measurement (Figure 2i).

3.2 | Water contact angle

The separators were treated with air RF-plasma to improve surface wettability and hydrophilicity of their surfaces. The water contact angle measurement is one of the common and simple methods to ascertain the wettability of material surfaces. Table 1 and Figure 3 represent the values of the water contact angle of SC separator films. A significant decrease can be seen in the water contact angles of all samples after plasma treatment. The contact angle of Celgard 2400 separator decreased from 115.3 to 52.1°. For the NKK cellulosic separator film, the contact angle was 0° both before and after plasma

treatment, which indicates that this film has a superhydrophilic surface (Supporting Information). Superhydrophilic PLA surfaces (with water contact angle dropped from 82.4 to 0°) were obtained after air RF-plasma treatment for 60 s. The improved wettability was clearly observed for Celgard 2400 and PLA films after plasma treatment. This is attributed to the formation of an oxidized nanolayer and the introduction of polar functional groups onto the separator surfaces. The air RF-plasma treatment made the surface more hydrophilic, thus improving its wettability characteristics. Similar results were reported by Ren and his coworkers for PLA nonwo-ven fabrics.[32] Atmospheric dielectric barrier discharge (DBD) plasma was applied to improve the surface wettability of PLA fabrics. DBD plasma treatment for 90 s sharply decreased the water contact angle from 123 to 0° and resulted in super-hydrophilic PLA surfaces. The effect of plasma treatment on the water contact angle reduction was also observed in a polylactic acid/hydroxyapatite (PLA/HA) composite[33] and a porous poly(lactic-co-glycolic acid) scaffold.[34] Jabbarnia et al. fabricated an electrospun polyvinylidene fluoride/polyvinylpyrrolidone-based (PVDF/PVP) separator for an SC.[35] UV irradiation changed the surface wettability of PVDF/PVP nanofibers. The hydrophilic surface of the SC separator displayed improved wettability with a contact angle of 37°.

TABLE 1 Water contact angle values of separators before and after RF-plasma treatment

Samples	Before RF-plasma treatment	After RF-plasma treatment
Celgard 2400	115.3 ± 1.4	52.1 ± 2.3
NKK-MPF30AC	0.0	0.0
PLA	82.4 ± 2.2	0.0

3.3 | Water absorption test

The water uptake (WU) data of separator films at room temperature are presented in Figure 2. Since RF-plasma introduces more hydrophilic functional groups into separator films, the tests were performed for both non-RF-treated (Figure 4a) and RF-treated (Figure 4b) separator films. After soaking nontreated separator films in water for 72 hr, the water uptake values were found to be 34.7%, 17.1%, and 3.2% for NKK, PLA, and Celgard 2400, respectively (Figure 4a). A cellulose based NKK separator showed the highest water absorption by hydrophilic (—NH and —OH) functional groups. Obviously, the polypropylene based Celgard 2400, which has a hydrophobic main chain structure, possesses the lowest water uptake value and low wettability. After the RF-treatment of separator films, the water uptake values increased to 186.6%, 149.9%, and 4.1% in RF-NKK, RF-PLA, and RF-Celgard 2400, respectively (Figure 4b). As expected, NKK and PLA separator films can absorb a huge amount of water after RF-treatment due to the surface modification toward a more hydrophilic character. There is a good correlation between the water uptake of all separator films and their water contact angle. One can see that there is a small increase in water uptake (from 3.2 to 4.1%) of the Celgard 2400 separator film after RF-treatment. This is attributed to the nonporous structure of the Celgard 2400 separator film. The porosity of the separator is crucial to achieve a higher aqueous electrolyte uptake and, consequently, improved ion transfer. Highly porous structures of NKK and PLA separators were also confirmed by SEM analysis.

In Figure 4b, all samples reach a maximum water uptake within 8 hr, followed by a gradual decrease until an equilibrium is reached. This behavior is called the overshooting phenomenon. Initially, water

diffuses into the porous films very rapidly. Then, polymer chains relax to their equilibrium conformations and release some amount of water. Similar behavior of sodium alginate-g-acrylic acid copolymer was reported in the literature.[36]

3.4 | ATR-FTIR analysis

The changes of the surface functional groups of separators were monitored by ATR-FTIR spectroscopy before and after RF air plasma treatment. Figure 5a,b is related with untreated and RF air plasma treated Celgard 2400 separator film.

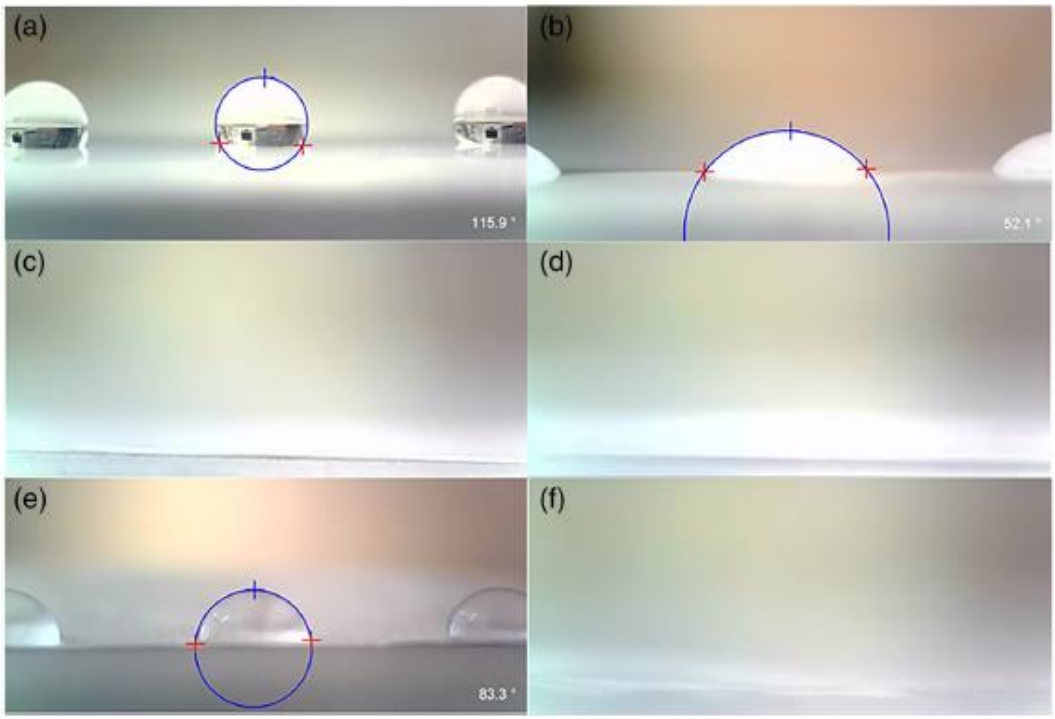

FIGURE 3 (a) Water contact angle images of Celgard 2400 before RF-treatment, (b) water contact angle images of Celgard 2400 after RF-treatment, (c) NKK-MPF30AC before RF-treatment, (d) NKK-MPF30AC after RF-treatment, (e) PLA before RF-treatment, and (f) PLA after RF-treatment [Color figure can be viewed at wileyonlinelibrary.com]

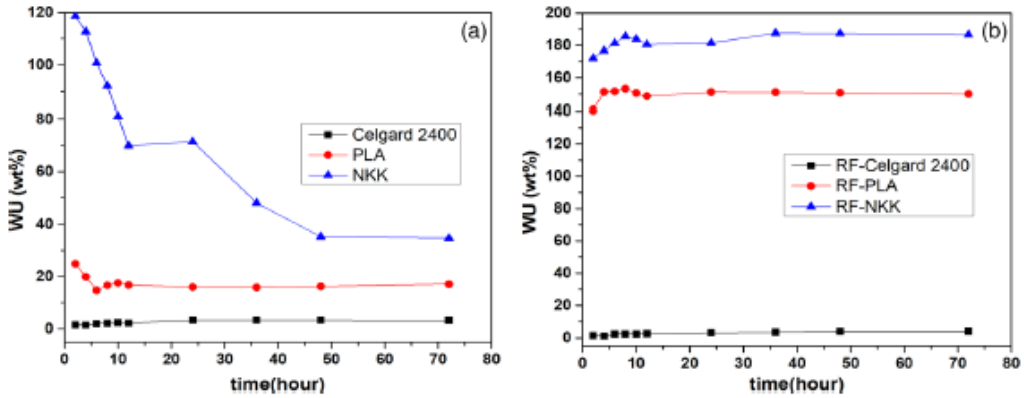

FIGURE 4 (a) WU% values before RF-treatment, (b) WU% values after RF-treatment [Color figure can be viewed at wileyonlinelibrary.com]

The strong peaks between 2,953 and 2,837 cm^{-1} are attributed to the —CH3 and —CH2 asymmetric and symmetric stretching vibrations. The two peaks at 1,456 and 1,372 cm^{-1} correspond to the asymmetric and symmetric deformation vibrations of —CH2 and —CH3, respectively. The medium peak at 1,166 cm^{-1} showed the C—H wagging vibrations and C—C bending of polypropylene. The —CH3 rocking can be seen clearly at 973 cm^{-1}. Researchers have used air plasma technique for modification of the polypropylene surface by incorporating hydrophilic oxidative functional groups, for example, carboxyl (—C=O—O—H), carbonyl (—C=O), and hydroxyl (—OH).[37] The formation of the oxygen containing functional groups on the surface of RF air plasma treated Celgard 2400 was confirmed by the FTIR spectrum given in Figure 4b. The new peak at 1,726 cm^{-1} is due to carbonyl (—C=O) groups stretching. Also, —O—H stretching and bending vibrations were identified as small peaks appeared at 3,441 and 1,621 cm^{-1}, respectively. The FTIR spectra of pristine and plasma treated NKK cellulose separator paper are presented in Figure 5c,d. The characteristic stretching vibrations of —CH2 groups were observed at 295,7 cm-1 and 2,917 cm^{-1}. The small peak at 1,734 cm^{-1} was observed for —C=O stretching vibration. The peaks at 1,456, 1,376, 1,162, and 994 cm^{-1} correspond to the —CH2 bending; —CH bending; C—O—C stretching; and ring vibrations of C—C, C—OH, and C—H groups, respectively.[38,39] The treated NKK surface showed almost same absorption peaks as the FTIR spectrum of untreated film. The only difference can be found as the increase in the peak intensity which corresponds to the carbonyl (—C=O) groups stretching at 1,734 cm^{-1}. The carbonyl peak intensity increment can be explained by addition of more hydrophilic oxidative functional groups onto the surface of NKK cellulose film by RF air plasma. The FTIR spectroscopic investigation was done for untreated and RF air plasma treated PLA films (Figure 5e,f).

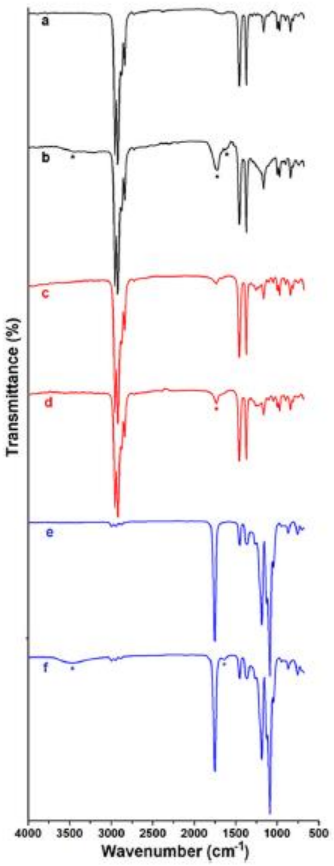

FIGURE 5 (a) FTIR spectra of Celgard 2400, (b) FTIR spektra of RF-Celgard 2400, (c) FTIR spectra of NKK-MPF30AC, (d) FTIR spectra of RF-NKK-MPF30AC, (e) FTIR spectra of PLA, and (f) FTIR spectra of RF-PLA [Color figure can be viewed at wileyonlinelibrary.com]

The typical absorption peaks of PLA at 2,998, 1,754, 1,453, 1,367 cm^{-1} were assigned to the —CH stretching in —CH_3 groups, —C=O stretching, asymmetric, and symmetric —CH bending in —CH_3 group, respectively. The strong peaks at 1,187 and 1,086 cm^{-1} were due to the C—O and C—O—C stretching vibrations. The oxidation of PLA with oxygen after plasma treatment was explained by the reaction of oxygen and free radicals to form peroxide groups in literature.[33,40] The proposed mechanism of the formation of peroxides was explained as the ejecting the hydrogen atom from —CH_3 group with the production of free radicals and subsequently react with O_2 to create peroxides and hydroperoxides.[41] The clear differences were observed for the RF air plasma treated PLA film in Figure 4f. The new peaks appeared at 3,469 and 1,637 cm^{-1} were related to the stretching and bending vibrations of the newly formed —OH groups onto the PLA surface. Hence, ATR-FTIR analysis confirmed that the RF air plasma modified the surface of PLA into the more hydrophilic character.

3.5 | Dielectric properties of separators

Figure 6 shows the frequency dependence of the complex permittivity of commercial separators NKK-MPF30AC and Celgard 2400 before and after RF plasma treatment.

All samples demonstrate frequency dispersion of permittivity in the studied frequency range. Plasma treatment has a pronounced effect on the dielectric properties of Celgard 2400 and PLA-based separators, but has little effect on the NKK separator. After plasma treatment, Celgard 2400 and PLA-based separators show an increase in the real part (dielectric constant) and imaginary part (dielectric losses). At the same time, the plasma treatment changes the character of the dielectric loss spectrum of both separators: the vanishing of β-relaxation in PLA at higher frequencies, and the vanishing of broad-band p-relaxation in Celgard 2400 in the low frequency region (Figure 6). This can be explained by the increase in the dipole polarizability due to the change in the surface chemical composition of the separators. Indeed, the surface of the PLA separator changes from hydrophobic to hydrophilic. The hydrogen atom in methyl groups (—CH_3) are likely to be removed and subsequently form radicals with the air oxygen, giving rise to hydroperoxides. After the plasma treatment, the chemical composition of the PLA separator surface is changed by incorporation of functional groups, for example, -C=O and —O—H; this leads to an increase in the number of dipoles in PLA.[42] These results are in a good agreement with the water contact angle and water uptake measurement results of the separators. Similar results were obtained for an oxygen plasma treated PVDF film: fluorine atoms were removed, radicals were formed, oxygen related functional groups were incorporated, and the PVDF film displayed improved hydrophilicity.[43] Table 2 presents the AC conductivity of separators before and after plasma treatment. The AC electrical conductivity of the separators increases slightly after the plasma treatment, but the separators still exhibit electrically insulating properties, which is what is expected for SC separators.

3.6 | Mechanical test

The stress-strain representative curves of the Celgard 2400, PLA, and NKK films are shown in Figure 7, and the film materials can be classified as brittle, plastic, and ductile, respectively. Their basic tensile properties are presented in Table 3.

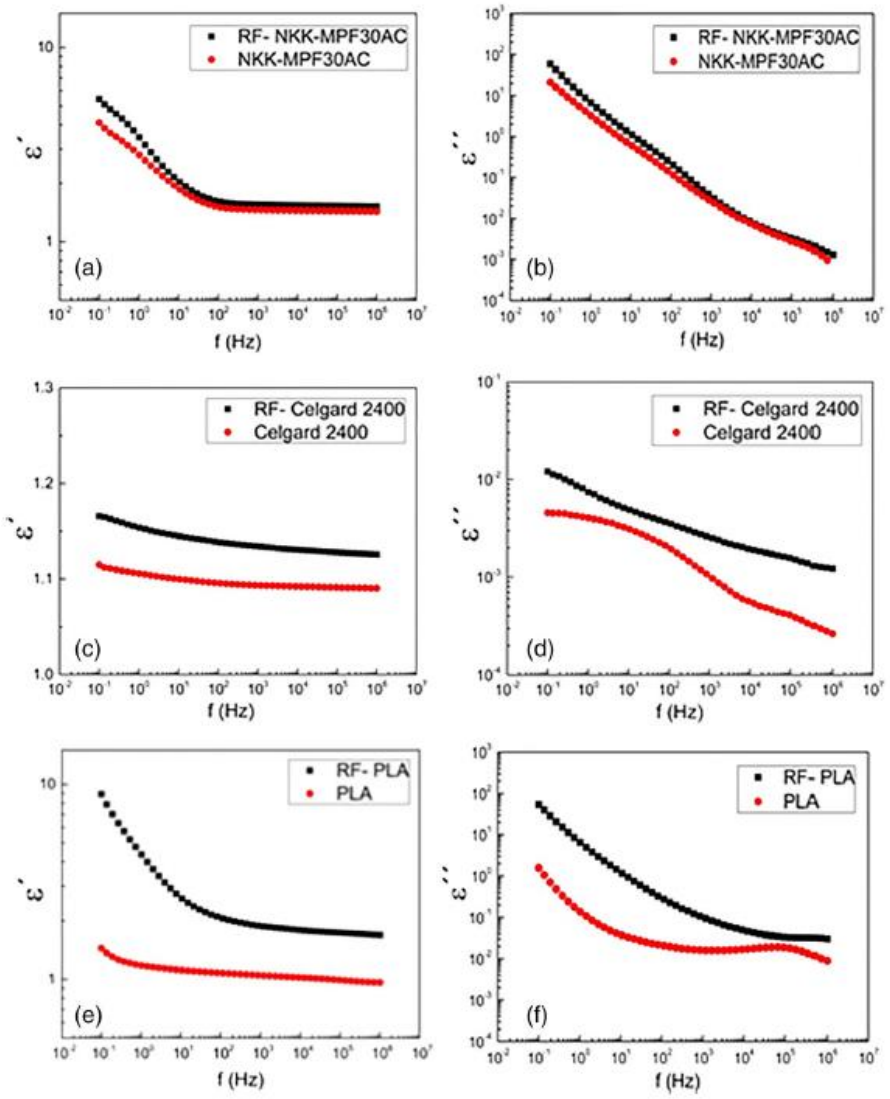

FIGURE 6 Dielectric spectra of commercial and PLA-based separators before and after RF plasma treatment [Color figure can be viewed at wileyonlinelibrary.com]

TABLE 2 AC conductivity of separators at frequency 100 Hz

Samples	σ_{AC} at 100 Hz
RF-Celgard 2400	$(3.47 \pm 1.60) \times 10^{-13}$
Celgard 2400	$(1.56 \pm 0.56) \times 10^{-13}$
RF-NKK-MPF30AC	$(1.19 \pm 0.10) \times 10^{-11}$
NKK-MPF30AC	$(5.68 \pm 1.25) \times 10^{-12}$
RF-PLA	$(1.77 \pm 0.08) \times 10^{-11}$
PLA	$(1.44 \pm 0.40) \times 10^{-12}$

It is shown that the RF-Celgard 2400 exhibits the highest ultimate tensile strength of 20.5 MPa and the highest Young's modulus of 481.6 MPa; however, it has the lowest elongation at break, 6.7%. This indicates that the RF-Celgard 2400 is a brittle material, as is shown in Figure 7. The RF-PLA has the second highest ultimate tensile strength of 15.2 MPa and a Young's modulus of 327.1 MPa. It has higher elongation at break (10.9%) than that of the RF-Celgard 2400. The mechanical properties of the RF-NKK-MPF30AC are different than those that it has the lowest ultimate tensile strength and Young's modulus, but the highest elongation at break. Thus it is a ductile but a low strength material compared to RF-Celgard 2400 and RF-PLA. It should be noted that the comparison of tensile test results is acceptable when the geometry of the samples for different materials is similar. Different thickness of samples can definitely affect the results of mechanical tests.[44] However, such comparison is possible in the case when for the same application is supposed to be used the different thickness for different materials with a view to achieve certain physical parameter. The results of tensile tests revealed that the RF-PLA separator has beneficial mechanical properties that allow it to withstand stress during assembly and operation.

3.7 | Electrochemical characterization

3.7.1 | Ionic conductivity

The electrolyte, that is, the electrolyte salt + solvent, is one of the key components of SCs. It provides ionic conductivity and thus facilitates the charge compensation on each electrode in the cell such as forming electric double layer (EDL) in capacitive behaviors and participating in the redox reactions of pseudocapcitors. Due to high ionic conductivity of strong acidic and alkaline electrolytes such as 1 M H_2SO_4 and 6 M KOH, they are widely used in EDLCs to achieve higher specific capacitance. Recently, neutral electrolytes such as 1 M Na_2SO_4 have drawn more attention in asymmetric SCs due to the wider work potential of electrodes in neutral electrolytes. Na_2SO_4 also has a superiority of noncorrosion to stainless steel current collector compared to Cl- containing electrolyte.[45] However, due to the decomposition of PLA in 6 M KOH, we have chosen two electrolytes for the separators, 1 M H_2SO_4 and Na_2SO_4, to test their performance

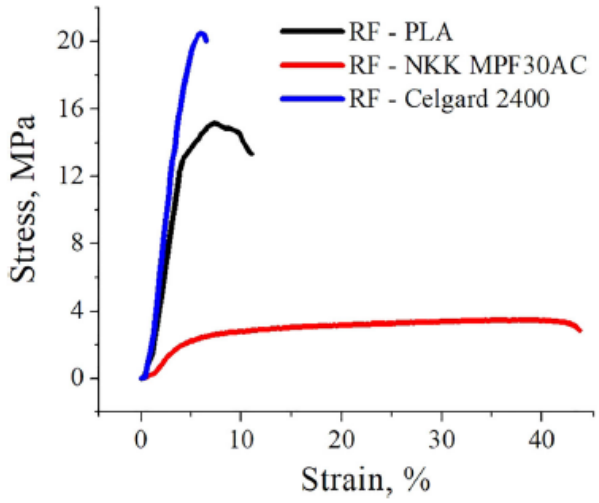

FIGURE 7 The stress-strain representative curves of RF-PLA, RF-NKK-MPF30AC, and RF-Celgard 2400 films [Color figure can be viewed at wileyonlinelibrary.com]

Table 4 shows the ionic conductivities of various separators in 1 M H2SO4 and 1 M Na2SO4. It was found that RF plasma treated samples have higher ionic conductivity in both electrolytes due to their improved hydrophilic-ity and that samples in 1 M H2SO4 have higher ionic conductivity than those in 1 M Na2SO4. Among them, RF-PLA in 1 M H2SO4 exhibits the second highest ionic conductivity of 1.1 x 10-1 S/cm, which is comparable to that of RF-NKK-MPF30AC (1.3 x 10-1 S/cm), which is attributed to its hydrophilicity and highly interconnected porous structure.

TABLE 3 Mechanical properties of Celgard 2400, NKK-MPF30AC, and polylactic acid samples

Samples	Thickness (μm)	Young's modulus (MPa)	Elongation at break (%)	Stress at break (MPa)	Ultimate strength (MPa)
RF-Celgard 2400	25 ± 0.8	481.6 ± 56.6	6.7 ± 1.6	19.8 ± 2.3	20.5 ± 2.1
RF-NKK-MPF30AC	30 ± 0.7	62.7 ± 15.4	44.2 ± 6.5	2.7 ± 0.6	3.3 ± 0.8
RF-PLA	44 ± 0.7	327.1 ± 64.2	10.9 ± 2.4	13.2 ± 1.4	15.2 ± 1.9

TABLE 4 Ionic conductivities of various separators in 1 M H_2SO_4 and 1 M Na_2SO_4, respectively

Samples	Electrolyte	Thickness (d) μm	Bulk resistance (R_b) Ω	Ionic conductivity (σ) S cm^{-1}[a]
NKK-MPF30AC	1 M H_2SO_4	34	0.24	0.7×10^{-1}
RF-NKK-MPF30AC	1 M H_2SO_4	34	0.132	1.3×10^{-1}
Celgard 2400	1 M H_2SO_4	24	30.9	3.9×10^{-4}
RF-Celgard 2400	1 M H_2SO_4	24	4.1	2.9×10^{-3}
PLA	1 M H_2SO_4	22	0.134	0.8×10^{-1}
RF-PLA	1 M H_2SO_4	22	0.096	1.1×10^{-1}
NKK-MPF30AC	1 M Na_2SO_4	34	0.23	0.5×10^{-1}
RF-NKK-MPF30AC	1 M Na_2SO_4	34	0.303	0.7×10^{-1}
Celgard 2400	1 M Na_2SO_4	24	39.4	3.0×10^{-4}
RF-Celgard 2400	1 M Na_2SO_4	24	2.8	0.4×10^{-3}
PLA	1 M Na_2SO_4	22	0.27	0.4×10^{-1}
RF-PLA	1 M Na_2SO_4	22	0.169	0.65×10^{-1}

[a] *The contact area between the stainless steel and separator (A) is a constant of 2 cm^2*

3.7.2 | Electrochemical performance of

Activated carbons are the most widely used materials for SCs because of their high specific surface area and moderate cost. Using activated carbon as active materials, SCs store charge electrostatically using reversible adsorption of ions of the electrolyte onto the surface of activated carbon, which is as called as EDLCs.[46] A typical CV of a two-electrode EDLC has a rectangular shape as these of RF-NKK-MPF30AC and RF-PLA in Figure 8. However, the CV of RF-Celgard 2400 has a spindle-like shape, which indicates that the formation of EDL is postponed owing to the limited ion mobility by the RF-Celgard 2400.

Figure 9 shows the CV curves of supercapacitors with different separator at various scan rates between 10 and 90 mV/s. The dependence of their current density on scan rate is summarized in the following graphs. Since there are no anodic or cathodic peaks in EDLCs, the current densities were selected at a potential of 0.8 V for charging and of 0.2 V for discharging. Typically, EDL capacitance formed via the reversible adsorption of ions on the surface of active electrode materials

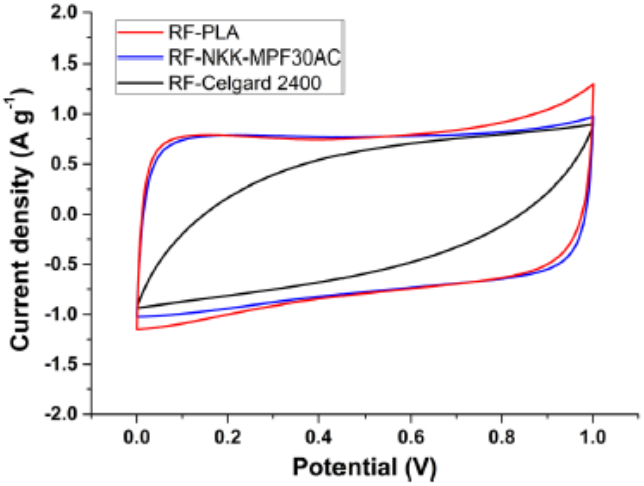

FIGURE 8 Cyclic voltammograms at scan rate of 20 mV/s of assembled supercapacitors with RF treated separators (RF-NKK-MPF30AC, RF-PLA, and RF-Celgard 2400) and activated carbon electrodes in 1 M H_2SO_4 [Color figure can be viewed at wileyonlinelibrary.com]

The capacitive current (i_c) from EDL capacitance has a linear dependence on the scan rate according to the equation: $i_c = AC_cv$, where C_c is the capacitance from capacitive process and A is a constant. This equation can be further simplified to $i_c = k_cv$, when all the reaction conditions are fixed except the scan rate. [47-50] Indeed, in the cases of RF-NKK-MPF30AC and RF-PLA, it displays a typical linear relationship, indicating the pure capacitive behavior without ions diffusion control. The *b*-values (the slopes of fitting lines) of RF-PLA are both higher than these of RF-NKK-MPF30AC at 0.8 and 0.2 V, which indicates it has a better capacitive behavior. The reason might be related to the permeated active material in the fibrous network structure of cellulose fibers in RF-NKK-MPF30AC. However, for RF-Celgard 2400, it presents a linear relationship until the scan rate became larger than 50 mV/s, where indicate it started to be limited by ion diffusion due to the hydrophobicity and low water absorption of "RF-Celgard 2400" in aqueous electrolyte.

EIS is among the most common techniques for the investigation of supercapacitors. In the measurement, the supercapacitor is charged/discharged within a narrow amplitude around a given potential. Therefore, the frequency can be directly correlated with the potential scan rate in cyclic voltammetry.[51] At the high frequency region, the semicircle indicates the charge transfer resistance (R_{ct}) formed at the electrode/electrolyte interface. Then it is the Warburg impedance associated with the diffusion. At the low frequent region, it represents the capacitive behavior. Figure 10a displays the Nyquist plots of SCs with RF-NKK-MPF30AC, RF-PLA, and RF-Celgard 2400. The low ionic mobility passing through RF-Celgard 2400 makes it has the highest R_{ct} and longest Warburg impedance region among three EDLCs at high frequency region and reach capacitive region (-phase > 45°) at lowest frequency of 0.019 Hz compared to these of RF-PLA RF-NKK (0.79 Hz) and RF-PLA (0.63 Hz). The impedance behaviors of RF-PLA RF-NKK and RF-PLA (0.63 Hz) were very similar. However, the slope of RF-PLA was higher than the one of RF-PLA RF-NKK at the capacitive behavior region at low frequency, which indicates a better capacitive process at low scan rate. All these were correlated with the results of CV analysis.

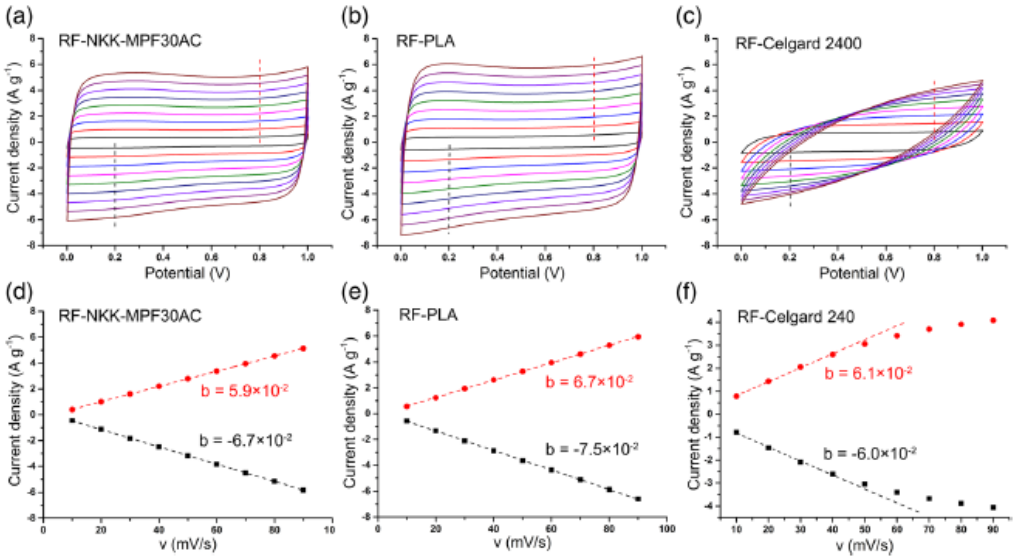

FIGURE 9 Cyclic voltammograms curves for scan rate from 10 to 90 mV/s of supercapacitors with (a) RF-NKK-MPF30AC, (b) RF-PLA, and (c) RF-Celgard 2400; the relationship between scan rate versus current density of each sample [Color figure can be viewed at wileyonlinelibrary.com]

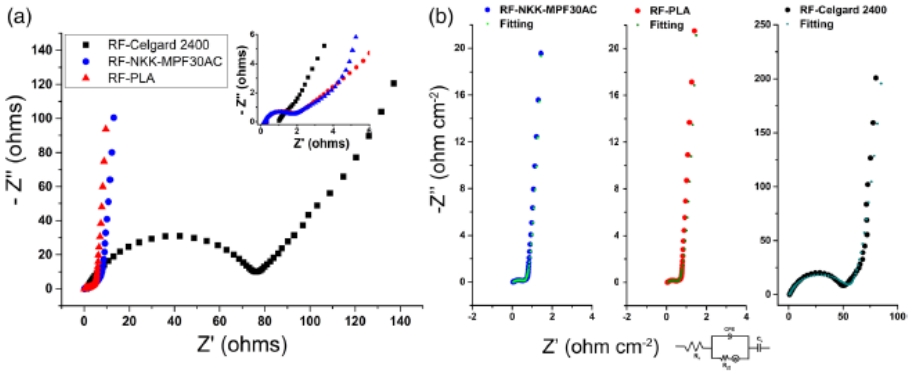

FIGURE10 (a) Nyquist plots of supercapacitors with RF-NKK-MPF30AC, RF-PLA, and RF-Celgard 2400 and (b) their fitting result by equivalent circuit model of $R_s(Q[R_{ct}\{W\}])C_L$ [Color figure can be viewed at wileyonlinelibrary.com]

TABLE 5 $R_s(Q[R_{ct}\{W\}])C_L$ equivalent circuit model parameter values for supercapacitors with RF-NKK-MPF30AC, RF-PLA, and RF-Celgard 2400, respectively

Parameter	RF-NKK-MPF30AC	RF-PLA	RF-Celgard 2400
R_s ($\Omega \times cm^{-2}$)	5.33×10^{-2}	6.23×10^{-2}	0.77
CPE; Y_o ($S\ s^{-n} \times cm^{-2}$)	1.74×10^{-2}	1.29×10^{-2}	1.29×10^{-2}
n	0.62	0.67	0.75
R_{ct} ($\Omega \times cm^{-2}$)	0.6	0.54	54.1
W; Y_o ($S\ s^{-0.5} \times cm^{-2}$)	1.95×10^{2}	1.99×10^{2}	9.26×10^{-2}
C_L ($F\ cm^{-2}$)	2.71×10^{-1}	3.13×10^{-1}	0.96×10^{-1}

The $R_s(Q[R_{ct}\{W\}])C_L$ equivalent electrical circuit model was given on the bottom of Figure 10b for the fitting analysis of the impedance data of RF-NKK-MPF30AC, RF-PLA, and RF-Celgard 2400 using ZSimpWin program. [52-54] The electrochemical parameters obtained from fitting the impedance data by the given circuit are shown in Table 5. In the circuit, R_s represents the solution resistance, R_{ct} is the charge transfer resistance, C_L is the capacitance at low at low frequencies, W is Warburg impedance, which shows the ion diffusion and CPE is the constant phase element (Q). [55] The highest solution resistance (R_s) was found as $R_s = 0.77\ \Omega/cm^2$ for RF-Celgard 2400 compared to $R_s = 5.33 \times 10^{-2}\ \Omega/cm^2$ for RF-NKK-MPF30AC and $R_s = 6.23 \times 10^{-2}\ \Omega/cm^2$ for RF-PLA. It was also clear that RF-Celgard 2400 obtained the highest the charge transfer resistance (R_{ct}). The highest capacitance (C_L) was obtained as $C_L = 3.13 \times 10^{-1}\ F/cm^2$ for RF-PLA, which was consistent with the result in CV analysis.

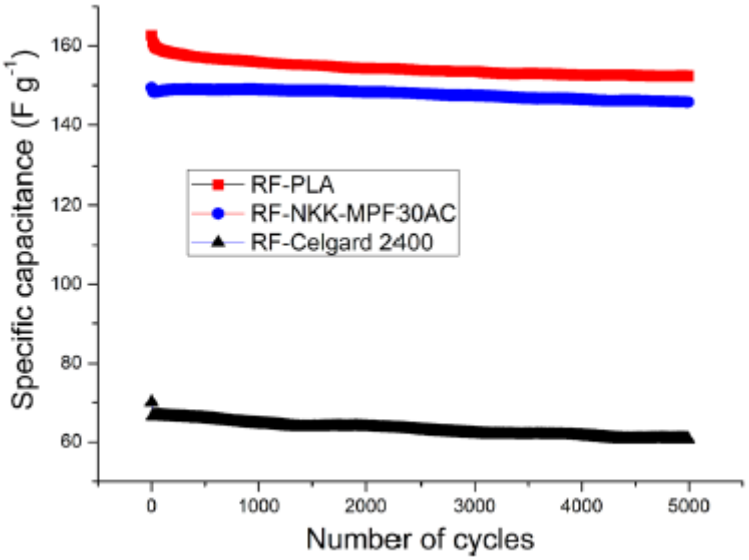

FIGURE 11 Cycling life of assembled supercapacitors with RF-NKK-MPF30AC, RF-PLA, and RF-Celgard 2400 [Color figure can be viewed at wileyonlinelibrary.com]

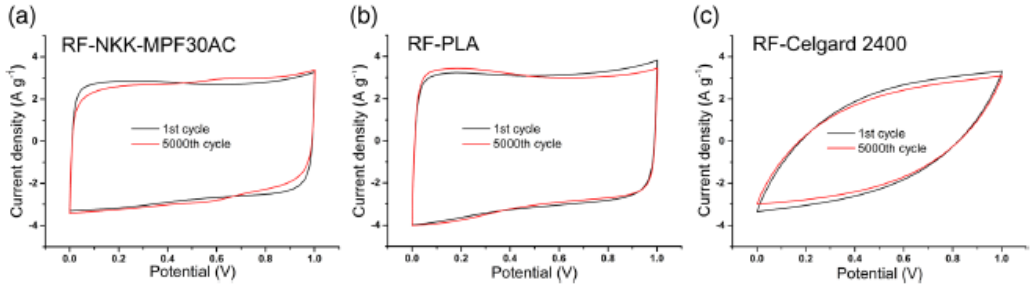

FIGURE 12 Cyclic voltammograms curves before and after cycling of supercapacitors with (a) RF-NKK-MPF30AC, (b) RF-PLA, and (c) RF-Celgard 2400 at scan rate of 50 mV/s [Color figure can be viewed at wileyonlinelibrary.com]

In order to reduce the effect of the electrode material on the cycling life of the SC, the EDLC cell was assembled using stable activated carbon as the electrode material and tested in a narrow potential window of 0.8 V. Figure 11 shows the cycling life of EDLCs of all separators, that is, RF-Celgard 2400, RF-NKK-MPF30AC, and RF-PLA. Both RF-NKK and RF-PLA have a good cycling stability of 97.5 and 93.7%

after 5,000 cycles at 1 A/g, respectively, while RF-Celgard 2400 has only 86.6%. It is because the polarization caused by the low ionic mobility in RF-Celgard 2400 might leads to the degradation of the active materials. CV measurements were conducted to compare the electrochemical behaviors before and after the cycling. The results are present in Figure 12. For all three samples, there were only slight changes on the shape of CV curves, which indicates that there were only limited degradation occurring during the cycling. All the separators exhibit good stability in the 1 M H2SO4 electrolyte, which is correlated with the SEM results for the morphology changes before and after cycling. Throughout the electrochemical measurements, RF-PLA has a performance comparable to that of RF-NKK-MPF30AC but much better than that of RF-Celgard 2400.

4 | CONCLUSIONS

Porous PLA films were prepared via phase inversion by using a PLA:PEG polymer blend (25:75 wt%). The full removal of the PEG sacrificial polymer resulted in PLA films with highly porous structure. All separators were subjected to RF-plasma treatment to obtain more hydrophilic surfaces. RF-plasma treatment not only improved the wettability but also increased the water uptakes of the NKK and PLA separator films. For PLA, the water contact angle decreased from 82.4 to 0°, and, for Celgard 2400, the water contact angle decreased from 115.3 to 52.1°. The contact angle of the NKK cellulosic separator film did not change upon RF plasma treatment, thus indicating its super hydrophilic surface. There was a small change in water uptake value (from 3.2 to 4.1%) of the Celgard 2400 separator after RF-treatment, but the water uptake of the PLA and NKK increased. The AC electrical conductivity of RF-PLA separator increases slightly after the plasma treatment, but it still exhibits electrically insulating properties, which is expected for SC separators. Moreover, PLA separator film exhibited a good mechanical resistance with tensile strength of 15.2 MPa, Young's modulus of 327.1 MPa despite its highly porous morphology. The SCs with an RF-PLA separator in electrolytes have ionic conductivity of about 1.1 X 10^{-1} S/cm. Its use in combination with activated carbon results in SC with typical EDLC behavior demonstrating a low internal resistance of 1.9 Ω and a good cycling life of 93.7% over 5,000 cycles.

REFERENCES

[1] D. P. Dubal, N. R. Chodankar, D.-H. Kim, P. Gomez-Romero, Chem. Soc. Rev. 2018, 47, 2065.

[2] A. González, E. Goikolea, J. A. Barrena, R. Mysyk, Renew. Sustain. Energy Rev. 2016, 58, 1189.

[3] D. D. L. Chung, Appl. Energy 2018, 231, 89.

[4] F. Wang, X. Wu, X. Yuan, Z. Liu, Y. Zhang, L. Fu, Y. Zhu, Q. Zhou, Y. Wu, W. Huang, Chem. Soc. Rev. 2017, 46, 6816.

[5] Z. Song, L. Li, D. Zhu, L. Miao, H. Duan, Z. Wang, W. Xiong, Y. Lv, M. Liu, L. Gan, J. Mater. Chem. A 2019, 7, 816.

[6] H. Peng, L. Xiao, K. Sun, G. Ma, G. Wei, Z. Lei, J. Power Sources 2019, 435, 226800.

[7] C. Chen, L. Hu, Acc. Chem. Res. 2018, 51, 3154.

[8] B. S. Noremberg, R. M. Silva, O. G. Paniz, J. H. Alano, J. Dupont, N. L. V. Carreflo, MRS Commun. 2019, 9(2), 726.

[9] C. Zhong, Y. Deng, W. Hu, J. Qiao, L. Zhang, J. Zhang, Chem. Soc. Rev. 2015, 44, 7484.

[10] Y. Guo, K. Zheng, P. Wan, Small 2018,14, 1704497.

[11] M. Zhou, H. Zhang, Y. Qiao, C. M. Li, Z. Lu, Cellulose 2018, 25, 3459.

[12] Y. Ji, N. Liang, J. Xu, D. Zuo, D. Chen, H. Zhang, Cellulose 2019, 26, 1055.

[13] L. Dagousset, G. Pognon, G. T. M. Nguyen, F. Vidal, S. Jus, P.- H. Aubert, J. Power Sources 2018, 391, 86.

[14] T. He, Y. Fu, X. Meng, X. Yu, X. Wang, Electrochim. Acta 2018, 282, 97.

[15] P. Huo, Z. Xun, S. Ni, Y. Liu, G. Wang, J. Gu, J. Appl. Polym. Sci. 2019, 136(30), 47759.

[16] Y. N. Sudhakar, M. Selvakumar, D. K. Bhat, Ionics 2013, 19, 277.

[17] Y. N. Sudhakar, M. Selvakumar, Electrochim. Acta 2012, 78, 398.

[18] M. F. Shukur, R. Ithnin, M. F. Z. Kadir, Electrochim. Acta 2014, 136, 204.

[19] P. S. Owuor, S. Inthong, S. M. Sajadi, P. Intawin, A. C. Chipara, C. F. Woellner, F. N. Sayed, H. H. Tsang, A. Stender, R. Vajtai, K. Pengpat, S. Eitssayeam, D. S. Galvao, J. Lou, C. S. Tiwary, P. M. Ajayan, Mater. Today Chem. 2019, 12, 132.

[20] P. Yang, J. Xie, C. Zhong, ACS Appl. Energy Mater. 2018, I, 616.

[21] Z. Peng, Y. Zou, S. Xu, W. Zhong, W. Yang, ACS Appl. Mater. Interfaces 2018,10, 22190.

[22] C. Chen, Y. Zhang, Y. Li, J. Dai, J. Song, Y. Yao, Y. Gong, I. Kierzewski, J. Xie, L. Hu, Energy Environ. Sci. 2017,10, 538.

[23] Q. Yao, H. Wang, C. Wang, C. Jin, Q. Sun, ACS Sustain. Chem. Eng. 2018, 6, 4695.

[24] J. Zeng, L. Wei, X. Guo, J. Mater. Chem. A 2017, 5, 25282.

[25] D. Zhao, C. Chen, Q. Zhang, W. Chen, S. Liu, Q. Wang, Y. Liu, J. Li, H. Yu, Adv. Energy Mater. 2017, 7, 1700739.

[26] Q. Xie, X. Huang, Y. Zhang, S. Wu, P. Zhao, Appl. Surf. Sci. 2018, 443, 412.

[27] C. O. Alvarez-Sanchez, J. A. Lasalde-Ramírez, E. O. Ortiz-Quiles, R. Massó-Ferret, E. Nicolau, Energy Sci. Eng. 2019, 7, 730.

[28] F. Kremer, A. Schonhals, Broadband Dielectric Spectroscopy, Springer-Verlag, Berlin Heidelberg 2003; Ch. 1, p. 3.

[29] R. D. Averett, M. L. Realff, K. Jacob, M. Cakmak, B. J. Yalcin, J. Compos. Mater. 2011, 45(26), 2717.

[30] Y. Chen, G. Xu, X. Liu, Q. Pan, Y. Zhang, D. Zeng, Y. Sun, H. Ke, H. Cheng, RSC Adv. 2018, 8, 39967.

[31] L. Tian, L. Xiong, X. Chen, H. Guo, H. Zhang, X. Chen, Materials 2018, 11(10), 1814.

[32] Y. Ren, L. Xu, C. Wang, X. Wang, Z. Ding, Y. Chen, Appl. Surf. Sci. 2017, 426, 612.

[33] O. Laput, I. Vasenina, M. C. Salvadori, K. Savkin, D. Zuza, I. Kurzina, J. Mater. Sci. 2019, 54, 11726.

[34] P. Liu, L. Sun, P. Liu, W. Yu, Q. Zhang, W. Zhang, J. Ma, P. Liu, J. Shen, J. Mater. Chem. B 2018, 6, 7605.

[35] A. Jabbarnia, W. S. Khan, A. Ghazinezami, R. Asmatulu, J. Appl. Polym. Sci. 2016, 133, 43707.

[36] Y. Yin, X. Ji, H. Dong, Y. Ying, H. Zheng, Carbohydr. Polym. 2008, 71, 682.

[37] R. Morent, N. De Geyter, C. Leys, L. Gengembre, E. Payen, Surf. Interface Anal. 2008, 40, 597.

[38] M. Fan, D. Dai, B. Huang, in Fourier Transform—Materials Analysis (Ed: S. M. Salih), InTech, London, UK, 2012; Ch. 3, p. 45.

[39] Y. P. Yang, Y. Zhang, Y. X. Lang, M. H. Yu. IOP Conf Series: Materials Science and Engineering, Guangzhou, China, 23-25 May 2017, 213, 012039.

[40] J. L. Shohet, Ch. 1. in Encyclopedia of Plasma Technology— Two Volume Set, CRC Press: Taylor & Francis, New York 2016, p. 38.

[41] J. Friedrich, The Plasma Chemistry of Polymer Surfaces: Advanced Techniques for Surface Design, Wiley, New York 2012, p. 21.

[42] P. Cools, N. De Geyter, R. Morent, Ch. 3. in PLA Enhanced via Plasma Technology: A Review, New Developments in Polylactic Acid Research (Ed: C. Winthrop), Nova Science Publishers, New York 2015, p. 79.

[43] D. M. Correia, J. Nunes-Pereirac, D. Alikin, A. L. Kholkin, S. A. C. Carabineiro, L. Rebouta, M. S. Rodrigues, F. Vaz, C. M. Costa, S. Lanceros-Méndez, Polymer 2019, 169, 138.

[44] E. O. Carew, J. Patel, A. Garg, P. Houghtaling, E. Blackstone, I. Vesely, Ann. Biomed. Eng. 2003, 31(5), 526.

[45] G. Monrrabal, B. Ramírez-Barat, A. Bautista, F. Velasco, E. Cano, Metals 2018, 8(7), 500.

[46] L. L. Zhang, X. S. Zhao, Chem. Soc. Rev. 2009, 38, 2520.

[47] F. Guo, N. Gupta, X. Teng, Ch. 5. in Supercapacitors— Theoretical and Practical Solutions, Intech Open, London 2018, p. 91.

[48] O. Capron, R. Gopalakrishnan, J. Jaguemont, P. Van Den Bossche, N. Omar, J. Van Mierlo, Materials 2018,11, 176.

[49] Y. Wang, D. Zhou, D. Zhao, M. Hou, C. Wang, Y. J. Xia, Elec-trochem. Soc. 2013, 160(1), 98.

[50] S. Zhu, X. Geng, Y. Han, M. Benamara, L. Chen, J. Li, I. Bilgin, H. Zhu, NPJ Comput. Mater. 2017, 3, 41.

[51] A. Eftekhari, J. Mater. Chem. A 2018, 6(7), 2866.

[52] S. Zhu, X. Sun, X. Gao, J. Wang, N. Zhao, J. Sha, J. Electroanal. Chem. 2019, 855, 113627.

[53] N. H. Basri, M. Deraman, M. Suleman, N. S. M. Nor, B. N. M. Dolah, M. I. Sahri, S. A. Shamsudin, Int. J. Electrochem. Sci. 2016,11, 95.

[54] S. Fletcher, V. J. Black, I. Kirkpatrick, J. Solid State Electro-chem. 2014,18, 1377.

[55] M. Ates, Y. N. Ertas, M. A. Serin, I. Ekmen, Polym. Bull. 2015, 72, 2573.